Energy 347 (2026) 140308

Contents lists available at ScienceDirect

Energy

journal homepage: www.elsevier.com/locate/energy

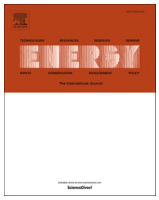

From ocean motion to green fuel: Integration of hybrid wave-tidal energy and offshore hydrogen production

Peihao Chen [a,*], Yan Zhang [a], Saeed Harati [b], Sara Walker [b], Karl Dearn [a]

[a] School of Engineering, University of Birmingham, Birmingham, B15 2TT, United Kingdom
[b] School of Chemical Engineering, University of Birmingham, Birmingham, B15 2TT, United Kingdom

ARTICLE INFO

Keywords:
Hydrogen generation
PEM electrolyzer
Wave energy
Tidal energy
Hydrogen integration
Co-simulation

ABSTRACT

Wave and tidal energy are promising renewable resources for offshore electricity generation, with hydrogen serving as a storable and transportable energy carrier. This study presents an integrated offshore hydrogen production system combining full-scale hybrid wave-tidal energy converters (HWTEC), hybrid supercapacitor-battery energy storage system, proton exchange membrane (PEM) electrolyzers, and subsea underground hydrogen storage (UHS). A system-level co-simulation framework is developed to capture the coupled dynamics of energy conversion, storage, and hydrogen production under stochastic marine conditions. UHS significantly reduces platform space requirements for hydrogen storage, enabling higher on-platform hydrogen capacity. A case study using 2024 UK wave and tidal data evaluates a conceptual platform with six HWTECs and PEM electrolyzers with combined average output of 64.8 kW. Results indicate a representative hydrogen production rate of 1.4 kg/h and an estimated annual yield of 12.4 t, with specific energy consumption of 46.8–55.7 kWh/kgH_2 and exergy efficiency of 21.4–25.3%. The system demonstrates enhanced power continuity, efficient conversion of intermittent offshore energy, and feasibility for grid-independent operation. The proposed framework advances beyond previous device-level studies by integrating multiple subsystems with real marine inputs, providing a scalable and practical tool for design, optimization, and performance assessment of offshore hybrid renewable hydrogen platforms.

1. Introduction

The transition toward carbon neutrality necessitates renewable energy systems that can deliver not only low-carbon energy but also high stability and operational efficiency. In this context, the integration of multiple renewable energy resources has attracted growing attention as an effective means to mitigate intermittency and improve overall system performance through resource complementarity [1], such as wind-solar, wave-wind, and thermal-wind combinations.

Within the marine environment, wave and tidal energy are particularly attractive owing to their high energy density, predictability, and comparatively continuous availability relative to solar and wind resources [2]. A wide range of wave energy converters (WECs) and tidal energy converters (TECs) have been developed [3,4]. Building upon these developments, hybrid wave–tidal energy converters (HWTECs) have been proposed to enhance energy capture and operational robustness by exploiting the complementary characteristics of wave and tidal resources. Chen and Wu [2] reviewed HWTEC concepts from the perspectives of system design and modeling approaches, categorizing them into non-coupling and coupling configurations based on the interaction between wave and tidal modules. Non-coupling systems typically operate in multiple modes or employ independent modules [5–7]. In contrast, coupling systems seek functional interaction between wave and tidal components to improve power smoothing and energy utilization. Examples include wave–current hybrid systems using mechanical motion rectifiers to preferentially harvest higher-speed inputs [8,9], as well as designs that combine swinging plates with horizontal cylinders [10] or integrate oscillating surge converters with buoys [11] to extend stroke length and enhance power output. More advanced coupling mechanisms, such as motion synthesis and resonance tuning, have also been explored to improve conversion efficiency and stability [12,13]. Nevertheless, most existing HWTEC designs still prioritize dominant inputs, often underutilizing the full complementary potential of wave and tidal resources. As noted by Chen and Wu [2], although effective wave–tidal coupling could significantly enhance complementary power generation, systematic design strategies and performance

* Corresponding author.
E-mail address: pxc249@student.bham.ac.uk (P. Chen).

https://doi.org/10.1016/j.energy.2026.140308
Received 9 December 2025; Received in revised form 14 January 2026; Accepted 1 February 2026
Available online 3 February 2026

assessments remain limited.

In parallel, energy storage has emerged as a critical challenge for ocean energy systems. Direct grid connection is frequently impractical for offshore wave and tidal energy due to power intermittency, voltage fluctuations, and load regulation issues [14]. Among various storage options, hydrogen production via water electrolysis has gained increasing attention as a means of converting marine renewable energy into a storable and transportable energy carrier. Recent techno-economic analyses highlight that the levelized cost of hydrogen (LCOH) is highly sensitive to electrolyzer performance, discount rates, and, critically, the availability of large-scale hydrogen storage, underscoring the importance of coordinated system-level design in offshore hydrogen projects [15]. Consequently, integrating hydrogen production with offshore renewable energy systems, particularly wave and tidal energy, has been widely recognized as a promising pathway to enhance energy utilization in offshore environments [16]. Such integrated systems have been proposed for energy self-sufficiency and scheduling on offshore platforms and islands [17,18]. A comprehensive review by Taroual et al. [19] indicates that wave and tidal energy remain among the most cost-competitive marine renewable sources for offshore hydrogen production, with reported hydrogen production costs of approximately 2.0–3.0 EUR/kg under favourable conditions. Oni et al. [20] further suggest that continued advances in offshore renewable deployment and electrolyzer durability could reduce LCOH to 2.5–3.5 USD/kg by 2035. Similarly, Akdağ [21] demonstrated that marine current-driven PEM electrolysis could achieve long-term cost competitiveness, with projected LCOH reductions from approximately 8.9 USD/kg in 2024 to around 2.34–2.365 USD/kg by 2050.

From an infrastructure perspective, recent studies emphasize a shift toward modular and decentralized offshore hydrogen platforms. An increasing number of studies have investigated the integration of ocean energy with hydrogen production [22,23], as summarized in Table 1. However, most existing studies treat energy capture, energy storage, and hydrogen production as loosely coupled or sequential modules, with limited emphasis on dynamic interactions and coordinated co-simulation. Moreover, operational constraints of PEM electrolyzers, such as minimum voltage and power thresholds [24], further complicate their integration with intermittent marine energy sources. In particular, systematic investigations that explicitly integrate hybrid wave-tidal energy with hydrogen production under realistic ocean conditions remain scarce.

Offshore hydrogen storage is likewise an essential aspect that cannot be overlooked. Meharban et al. [33] and Pham et al. [34] demonstrate that repurposed oil and gas structures and floating renewable-based platforms can provide scalable solutions for exploiting distant offshore resources while avoiding the need for subsea power transmission. In parallel, national-scale demonstration projects in Germany, Japan, and China increasingly couple offshore renewables with PEM electrolyzers and large-scale hydrogen storage solutions, such as salt caverns and onboard compressed hydrogen systems, to mitigate intermittency and enhance supply stability under offshore conditions [15,35]. Collectively, these studies reveal a clear trend from isolated component-level optimization toward coordinated offshore system integration. However, systematic investigations of integrated offshore hydrogen platforms that explicitly couple wave and tidal energy with offshore hydrogen production remain largely unexplored, reinforcing the need for modeling frameworks that jointly consider energy conversion, hydrogen storage, and marine infrastructure constraints.

Despite growing interest, system-level modeling approaches capable of capturing the coupled dynamics and complexity of such integrated offshore systems remain insufficiently developed. Conventional modeling of WECs [36,37] and TECs [38,39] often relies on simplified representations, such as wave energy flux formulations, linear wave theory, or parameterized tidal power equations, which facilitate analytical treatment but inadequately represent real ocean dynamics [40,41]. PEM electrolyzer models commonly adopt macroscopic energy balance approaches [27,29], yet transient electrochemical responses under fluctuating power inputs are rarely addressed [42,43]. Although hydrodynamic time-domain simulations have been employed in some integration studies [44], and data-driven approaches have been explored for wind–hydrogen systems [45], most existing work continues to rely on generalized device behaviour and statistical representations. A significant limitation in current research is the lack of integrated co-simulation frameworks capable of capturing time-varying ocean energy inputs, battery energy buffer, dynamic response of PEM electrolyzers, and the coordinated operation of energy capture devices and storage systems. Such frameworks are particularly critical for hybrid wave–tidal systems, where multi-source fluctuations interact across subsystems, and are essential to accurately represent both individual device performance and system-level integration dynamics.

In summary, existing studies on offshore renewable hydrogen production still exhibit several critical limitations at the system-integration level. First, wave and tidal energy are typically treated as independent or weakly coupled resources, which limits the understanding of their coordinated contribution under realistic marine conditions. Second, many existing modeling approaches rely on idealized sea states or continuous input formulations, which are insufficient to represent the stochastic and intermittent nature of real ocean environments. More importantly, current studies largely focus on individual devices or isolated subsystems, and lack an integrated framework that simultaneously captures energy conversion, energy buffering, electrochemical hydrogen production, and storage constraints in a unified manner.

To address these gaps, this paper develops a system-level co-simulation framework for offshore hydrogen production powered by hybrid

Table 1
Summary of recent studies on ocean energy-hydrogen production system.

Team	System	Power capacity	H_2 production rate	Exergy efficiency	Energy efficiency
Sánchez-Dirzo et al. [25]	Blow-Jet WEC + PEM electrolyzer	0.37 W	7.37×10^{-6} kg/h	/	Current efficiency 88.99%~90.58%
Molina-Salas et al. [26]	Offshore OWC + PEM electrolyzer	Scale-dependent	/	30%~60%	/
Kenez and Dincer [27]	Offshore wind farm + PEM electrolyzer	2.0×10^7 W	360 kg/h (liquefied H_2)	Overall 7.95%	Overall 25.64%
Mehrenjani et al. [28]	Multi-source platform (ocean thermal, wind, solar)	1.43×10^5 W	3.96 kg/h	Overall 16.02%	/
Bekçi et al. [29]	Oscillating wave surge converter + PEM electrolyzer	1.0×10^5 W	0.38–0.39 kg/h	/	41.5–46.4 kW h/kgH_2
Kurniawan et al. [30]	OWC wave energy system	4.22×10^3 W (average)	0.07 kg/h	/	WEC 0%~20%, PEM electrolyzer 56%~77%
Ozturk & Dincer [31]	Integrated solar-wind-wave system	7.5×10^5 W	0.15 kg/h	/	/
Gursoy & Dincer [32]	Solar-ocean integrated plant	1.63×10^7 W (net power)	450 kg/h	16.61 %	15.83 %

wave-tidal energy. Building upon previously validated device-level modeling approaches, the proposed framework embeds a full-scale hybrid wave-tidal energy converter as one subsystem within a coupled system that integrates battery energy storage, PEM electrolysis, and hydrogen storage. Real stochastic wave and tidal data from UK offshore waters are directly incorporated, enabling long-term performance assessment under realistic operating conditions. Furthermore, by explicitly considering underground hydrogen storage potential, the proposed framework links marine energy conversion with offshore infrastructure constraints and platform configuration, allowing the impact of storage strategy on rated power design and hydrogen production capacity to be systematically evaluated. This integrated approach moves beyond scenario-based assembly of individual models and provides a holistic basis for the design and assessment of offshore hybrid renewable hydrogen platforms.

The rest of this paper is organized as follows: Section 2 briefly outlines the system architecture. Section 3 covers the HWTEC design and discretization nonlinear modeling with experimental validation. Section 4 presents the engineering-level PEM electrolyzer modeling. Section 5 details the system integration, performance evaluation and deployment case. Section 6 concludes the work.

2. System overview

The PEM electrolyzer hydrogen production system proposed for offshore platform in this study enables the conversion of ocean energy into electricity, which is then used to produce hydrogen via a PEM electrolyzer. This approach facilitates the transformation of ocean energy, typically challenging to store or transmit over long distances, into hydrogen, a more manageable and transportable energy carrier.

The system comprises two primary components: the HWTEC and the offshore platform (Fig. 1). The HWTEC consists of waterproof casing, buoy, turbine, nonlinear motion rectification and coupling device (NLMRCD), and generator. The offshore platform accommodates the supercapacitor module and battery, PEM electrolyzer, and hydrogen storage vessels. The HWTEC is deployed near the offshore platform. The buoy captures wave energy through vertical oscillation, while the turbine, guided by tail fins, aligns with tidal currents to extract tidal energy. These two energy sources are mechanically coupled via the NLMRCD, which rectifies and combines their motion into a unidirectional rotation to drive the generator. The generated electricity is transmitted through a short subsea cable to the offshore platform, where it is rectified and temporarily stored in the supercapacitor module and battery. These modules stabilize voltage and buffers power fluctuations, providing a steady power supply to the PEM electrolyzer. The electrolyzers use desalinated seawater as feedstock to produce hydrogen, which is then preliminarily compressed and stored in onboard hydrogen vessels. The oxygen byproduct can also be utilized to improve the system overall economic value.

The system design allows flexible scaling of both HWTEC units and hydrogen storage capacity, depending on the platform scale and function. Compared to direct electricity transmission, converting energy into hydrogen avoids long-distance transmission losses and infrastructure costs, offering a promising and adaptable solution for offshore renewable energy utilization.

3. Hybrid wave-tidal energy converter

A stable energy supply is essential for devices such as PEM electrolyzers, which are highly sensitive to voltage fluctuations. To meet this requirement, this study proposes the HWTEC as energy supply unit. It simultaneously harnesses tidal and wave energy, utilizing their complementary characteristics to reduce the intermittency and fluctuations of single-source energy.

3.1. NLMRCD design

As the core component of the HWTEC, the NLMRCD is designed to rectify reciprocating mechanical motions and enhance output speed (Fig. 2). It performs two key functions, mechanical motion rectification and motion coupling, through a rack-pinion mechanical motion rectifier (MMR) (Fig. 2a) and a bevel gearbox (Fig. 2b), respectively.

In the rack-pinion MMR (Fig. 2a), each gear mounted on the input shaft is fitted with a one-way bearing and referred to as a “one-way gear”

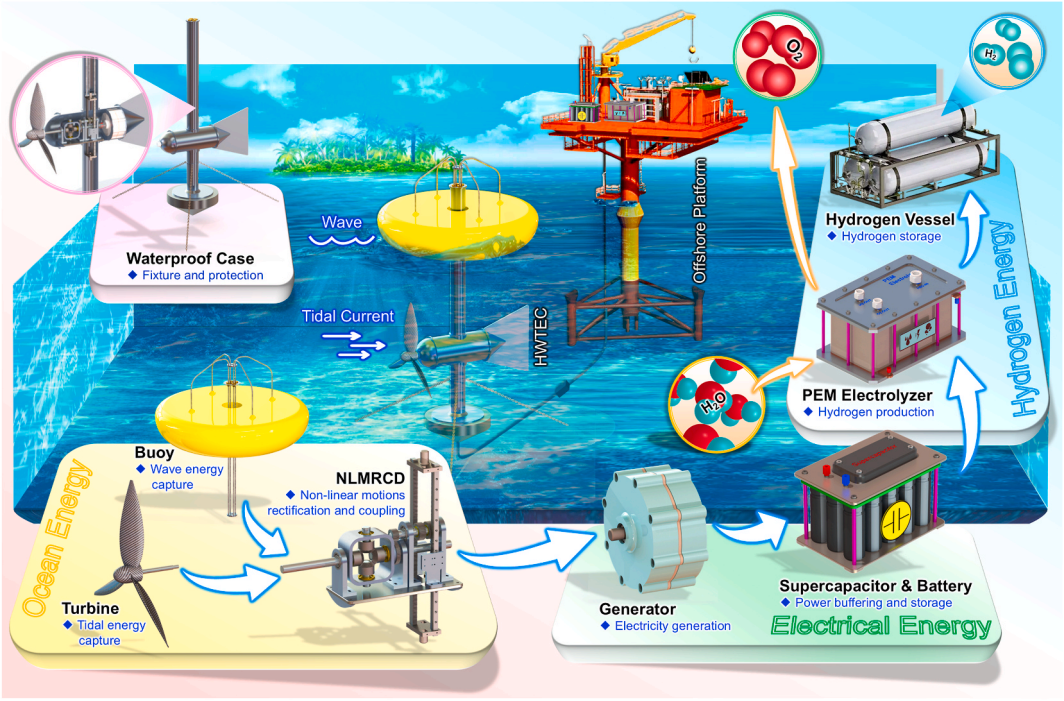

Fig. 1. Offshore platform PEM electrolyzer hydrogen production system powered by the hybrid wave-tidal energy converter.

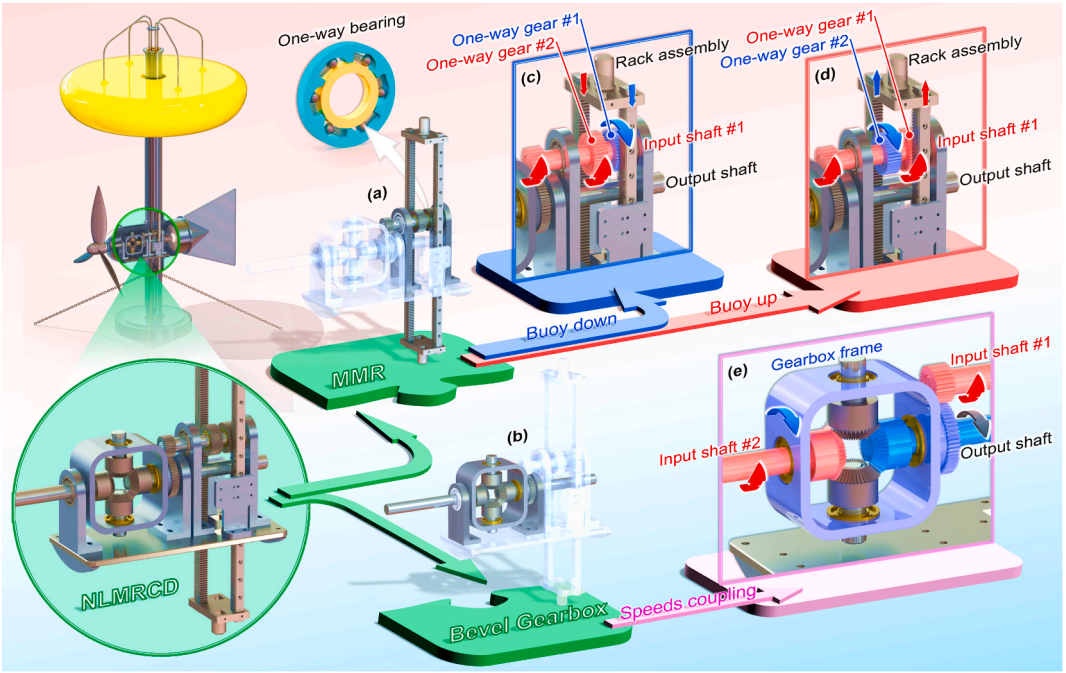

Fig. 2. Working principle of non-linear motions rectification and coupling device.

in this study. When the gear rotates in the engagement direction of the one-way bearing, the bearing locks the gear to the shaft, allowing synchronous rotation. Conversely, in the disengagement direction, the gear rotates independently of the shaft. Two such one-way gears, oriented identically, ensure that the input shaft rotates continuously in one direction despite being driven by the reciprocating motion of the rack assembly. Thus, this mechanism enables the oscillating vertical motion of the buoy driven by wave action to be rectified into continuous unidirectional rotation of input shaft #1.

Furthermore, one-way bearings exhibit an overrunning effect, allowing the driven shaft to continue rotating by inertia when the driving speed decreases. This not only reduces input power demand but also improves transmission efficiency. This design avoids mechanical jamming, reduces impact and energy losses from frequent directional switches, and significantly enhances transmission smoothness and efficiency. Due to the nonlinear feature of this transmission process, the overrunning effect requires special attention in system modeling.

The bevel gearbox (Fig. 2b) merges the unidirectional rotations from both the turbine and the MMR to generate the final output. The output is derived from the relative speed between these two inputs, which equals the sum of their individual speeds. Consequently, compared with devices that rely on a single input, the NLMRCD minimizes output speed reduction or interruption when one of the input speeds becomes weak or unstable.

In terms of system reliability, the mechanical complexity is not substantially higher than other wave and tidal energy converters [2]. Existing studies indicate that gear mechanisms under safe loads can achieve service lifespans comparable to those of wind turbines, even when considering the effects of seawater corrosion and extreme weather [46]. With regard to extreme offshore conditions, the design can incorporate protective features in deployment to prevent damage in storms.

3.2. Modeling methods

The modeling of HWTEC mainly includes two parts: the discretization modeling method and the pseudo real-time waves (PRTW) simulation.

Due to the incorporation of the overrunning effect and variable damping, the acceleration is no longer solely determined by the input force, it also depends on the current motion state of the driven components. This makes traditional continuity equation method for deriving acceleration functions inapplicable. In the discretization modeling method, the continuity equation is discretized by dividing velocity into small time increments (Δt) Between adjacent velocity points, a local linear approximation is defined, to determine the corresponding acceleration. Hence, the instantaneous motion state can be solved directly.

In addition, to enable automatic determination of the state switching between the overrunning phase (nonlinear) and the meshing phase (linear), specific boundary conditions are defined. The reciprocating motion of the buoy v_w is converted into unidirectional rotation of the one-way bearings ω_{in1} by the pinion-rack MMR. During overrunning, input shaft #1 rotates faster than the one-way gears, introducing an intermediate velocity variable ω'_{in1}. Key variables include input torque M_{in1}, damping torque M_{d1}, and equivalent moments of inertia of driving components and driven components J_1 and J_3. On tidal side, the tidal turbine input ω_{in2} and the final output angular velocity ω_{out} drive the generator. The boundary conditions for identifying the start of the overrunning effect can be expressed as,

$$\begin{cases} M_{mid} > 0 \\ \dfrac{M_{in1} - M_{mid} - M_{d1}}{J_1} = \dfrac{M_{mid} - M_{d3}}{J_3} \\ \omega_1 = \omega_1' \end{cases} \rightarrow \begin{cases} M_{mid} = 0 \\ \dfrac{M_{in1} - M_{d1}}{J_1} < \dfrac{-M_{d3}}{J_3} \\ \omega_1 = \omega_1' \end{cases} \tag{1}$$

and for the end of the overrunning effect is,

$$\begin{cases} M_{mid} = 0 \\ \dfrac{M_{in1} - M_{d1}}{J_1} > \dfrac{-M_{d3}}{J_3} \\ \omega_1 < \omega_1' \end{cases} \rightarrow \begin{cases} M_{mid} > 0 \\ \dfrac{M_{in1} - M_{mid} - M_{d1}}{J_1} = \dfrac{M_{mid} - M_{d3}}{J_3} \\ \omega_1 = \omega_1' \end{cases} \tag{2}$$

In Eqs. (1) and (2), angular velocity and acceleration are interdependent due to the presence of damping. By discretizing the input velocity, the angular velocities, accelerations and torque at each time step can be calculated sequentially and used to determine the values at the next step. Based on these above conditions, the equations of motion for

HWTEC input shaft #1 in meshing phase can be given as:

$$M_{in1} = (J_1\alpha_1 + J_3\alpha_3) + (c_1\omega_1 + c_3\omega_{out}) + (M_{d1} + M_{d3}) \tag{3}$$

while in overrunning phase, it is presented as,

$$\begin{cases} M_{in1} = J_1\alpha_1 + c_1\omega_1 + M_{d1} \\ 0 = J_3\alpha_3 + c_3\omega_{out} + M_{d3} \end{cases} \tag{4}$$

The equations of motion for HWTEC input shaft #2 is,

$$M_{in2} = J_2\alpha_2 + (c_2 + c_3)\omega_{out} + M_{d2} \tag{5}$$

where, M_{in2} represents the input torque of input shaft #2, while α_1, α_2 and α_3 denote the angular accelerations of input shaft #1, input shaft #2 and the output shaft. J_2 is the equivalent moment of inertia of the tidal-driving components. c_1 and c_2 are the viscous damping coefficients for the wave-driving components and tidal-driving components, respectively, whereas c_3 represents the electrical damping coefficient of the generator. Additionally, M_{d2} is damping torque acting on input shaft #2. The input torque M_{in1} on shaft #1 can be converted into the input force F_{in} from wave buoy, as follows,

$$M_{in1} = F_{in} \cdot r_{og} \tag{6}$$

where r_{og} is the radius of the one-way gear. The electrical damping torque M_e of the generator constitutes a significant portion in the damping torque M_{d3}.

$$\begin{cases} M_e = c_3\omega_{out} = \dfrac{k_t k_e \omega_{out}}{R} \\ U = k_e\omega_{out} \cdot \dfrac{R_{ex}}{R_{ex} + R_{in}} \end{cases} \tag{7}$$

where k_t and k_e are the torque coefficient and the back electromotive voltage coefficient of the generator. U is the output voltage. R_{in} and R_{ex} are the internal resistance and the external resistance in the circuit.

Preliminary simulations of the HWTEC, based on the above discretization modeling method and boundary conditions, reveal the effects of overrunning and wave-tidal coupling (Fig. 3). During the overrunning phase, the required wave input force drops sharply (Fig. 3a), while the minimum output voltage increases (Fig. 3c). The coupling mechanism slightly enhances tidal input torque (Fig. 3b), indicating improvement in energy extraction and rise in the voltage minimum (Fig. 3c). These combined effects help mitigate voltage interruptions, which is essential for stable offshore hydrogen production. Though a small time-step misalignment error of Δt is introduced, it simplifies the solution process and enables automated simulation. Validation against experimental results shows that with $\Delta t = 0.001$ s, the relative error remains within 0.5% [47].

The PRTW is introduced to address the lack of seconds-level wave data in open seas, and to provide discrete, random wave data input for validating the discretization modeling method. It is developed based on Random Wave Theory and the trochoid equation, to overcome the limitations of conventional sinusoidal wave assumptions and enhance wave modeling realism. Experimental observations indicate that trochoidal waveforms incorporating longitudinal motion more accurately represent real ocean conditions under wind influence [48]. In order to enhance simulation accuracy while ensuring computational efficiency, wave discretization is employed as a simpler and more direct alternative to Fourier transform or spectral methods, facilitating integration with the discretization HWTEC model. The Gerstner wave model describes water particle motion, capturing depth-dependent attenuation effects [48]. Wave-breaking conditions follow the theory of Stokes, where waves break when the wave steepness H/λ exceeds 1/7, and unbroken waves exhibit a crest angle exceeding 120°. Ocean conditions are typically characterized by the significant wave height $H_{1/3}$ and the average zero-crossing period T_z. In the Random Wave Theory [48], Rayleigh distribution effectively represents wave height distribution, while Gaussian distribution generates random wave heights in ocean simulations.

An analysis based on wave data at the selected site indicates that the daily average wave energy density over 2024 spans a wide range from 0.74 to 526.20 kW/m (Fig. 4a). By binning the daily wave energy density using a step size of 5 kW/m, the distribution of occurrence days is obtained (Fig. 4b). The results show that the most frequent energy density range in 2024 is 10~15 kW/m, occurring on 41 days, while energy densities between 5 and 20 kW/m account for a total of 111 days. Based on this distribution, May 17, with a daily-averaged wave energy density of 12.46 kW/m, which is close to the central value of the most frequently occurring range, is selected as a representative operating condition for device sizing and performance assessment. On this day, data from the National Data Buoy Center (Station 62050-E1, 50.0°N, 4.4°W) shows that the significant wave height ranged in 1.0–1.6 m, with a dominant wave period of 2~6 s. The scale parameter of the Rayleigh Distribution for significant wave height is set to 1.6 m. The PRTW generated from these parameters represents the instantaneous wave profile. By dividing this profile by the wave phase speed, the time-varying wave height at a fixed point can be obtained (Fig. 4c). Assuming the instantaneous position of the buoy approximates the local wave height, its velocity variation over time can be easily derived (Fig. 4d).

3.3. Simulation and experiments validation

A dual-input test bench (Fig. 5a) is established to validate the modeling and simulation. Two servo motors are employed to simulate the reciprocating motion of waves and the rotation of the tidal turbine, and a permanent magnet synchronous generator (PMSG). The parameters are listed in Table 2. Multiple repeated tests are conducted under various input conditions. These conditions include wave heights ranging from 40 to 160 mm, wave frequencies between 0.2 and 1.0 Hz, and tidal turbine speeds from 60 to 180 rpm [49].

As a representative case, the experimental results corresponding to tidal turbine speed of 60 rpm, wave frequency of 0.6 Hz, wave height of 100 mm, and external load of 498.7 Ω are presented in Fig. 4b–d and summarized in Table 3. Simulation results indicate that the overrunning phase accounts for 37.7% of the entire cycle. It is found that the simulation can accurately predict the dynamic behavior of the HWTEC, particularly the nonlinear response due to the overrunning effect.

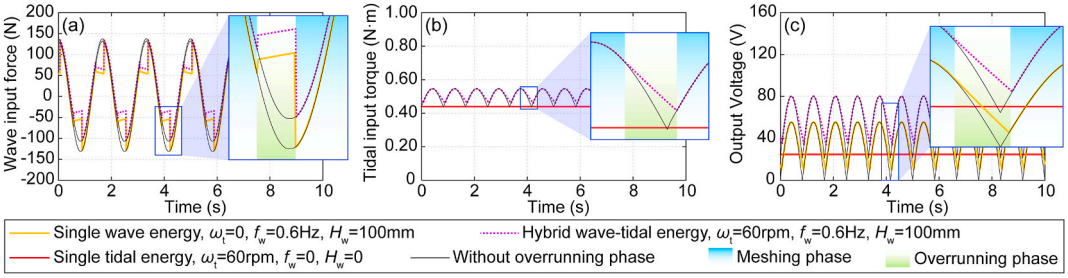

Fig. 3. Preliminary validation for nonlinear and coupling effect.

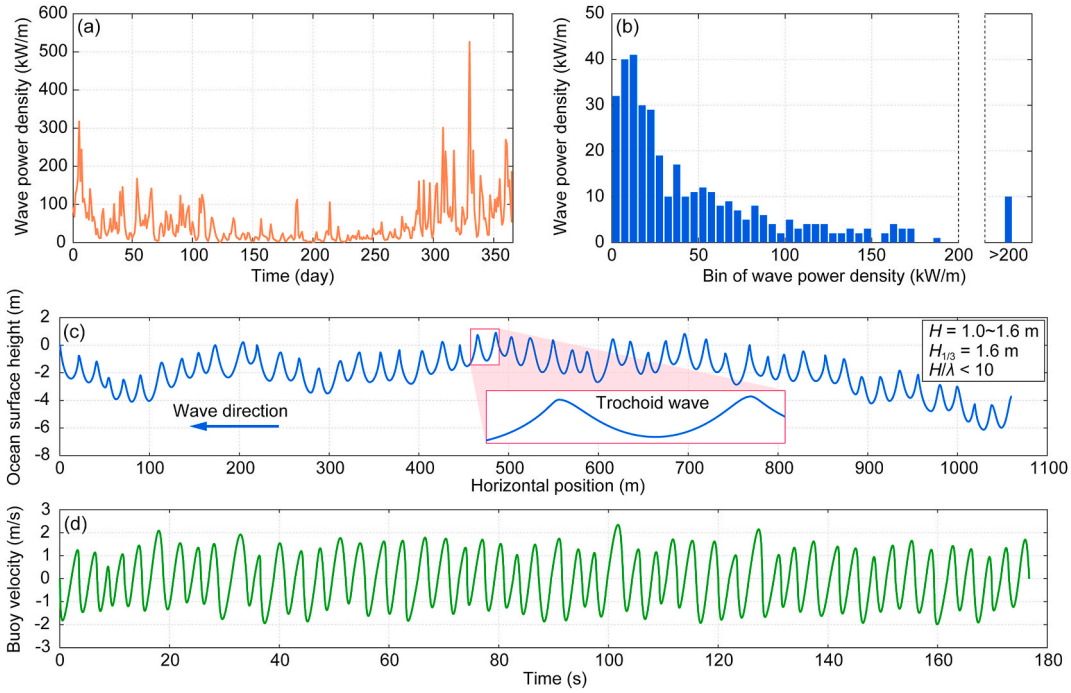

Fig. 4. Daily average wave energy density over 2024 and pseudo real-time waves (PRTW) generated.

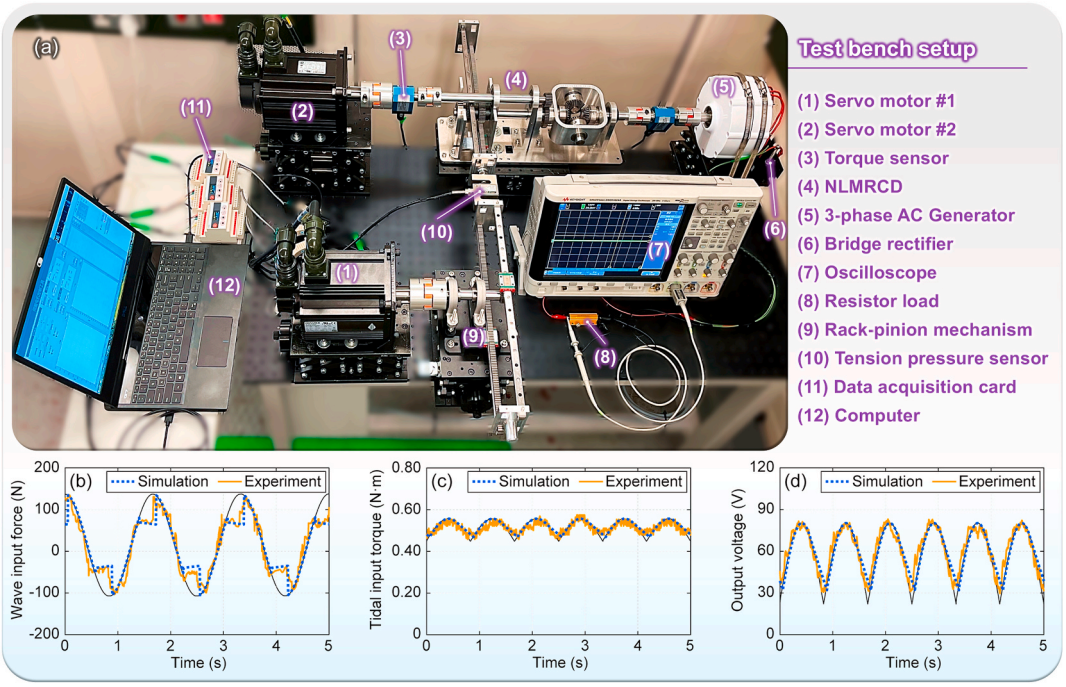

Fig. 5. Simulation and test validation. (a) Test bench setup. (b)~(d) Comparison of simulation results and experiment results.

Despite mechanical tolerances and system noise, the experimental data exhibit good agreement with simulation predictions, validating the validity and reliability of the modeling approach. It is also observed that the damping coupling introduces energy losses, causing a slightly lower overall efficiency of the HWTEC compared to single source wave or tidal energy converters. Nonetheless, the hybrid configuration enhances the energy capture capability through wave-tidal synergy. Notably, the concept of hybrid wave-tidal energy in increasing the minimum output voltage is preliminarily validated, underscoring its potential in offshore hydrogen production.

The prototype tests confirm the feasibility and accuracy of the discretization modeling. To further verify its applicability and generalization, simulations for energy converters of different scales in real ocean need to be conducted, where the lack of time series data with seconds resolution of waves in open sea needs to be addressed. Hence, PRTW is introduced to represent realistic sea states instead of the ideal sinusoidal input used in experiments, thereby enhancing the practical relevance of the simulation results [47]. The generated PRTW sequences are constructed under the assumption of a narrow-band, linear random sea state, which has been widely adopted as a first-order representation in

Table 2
Experiment setup parameters.

Generator type	PMSG	Gear ratio of tidal turbine - gearbox	1:2
Generator rated power	400 W	Gear ratio of wave racks - input shaft	1:1
Generator rated voltage	48 V	Servo motor rated power	3 kW
Generator rated speed	200 rpm	Servo motor rated torque	9.8 N m
AC/DC converter	Bridge rectifier	Servo motor torque constant	1.2 N m/A
Moment of inertia J_1 (mesh)	2.43×10^{-3} kg m^2	Servo motor rotor inertia	7.72 kg cm^2
Moment of inertia J_1 (overrun)	2.28×10^{-3} kg m^2	External resistor load	500 Ω
Moment of inertia J_2	1.02×10^{-4} kg m^2	Stroke of NMLRCD prototype	±100 mm
Moment of inertia J_3	2.81×10^{-4} kg m^2	External load resistance	498.7 Ω

Table 3
Results summary and comparison of simulation and experiment.

Result parameters	Simulation results	Experiment results
Average wave energy input power (W)	8.9	9.2
Average tidal energy input power (W)	3.5	3.5
Average output power (W)	6.1	6.4
Efficiency	49.3%	50.4%
Minimum output voltage (V)	32.5	28.4
Maximum output voltage (V)	79.2	82.0
Ratio of min-max voltage	41.0%	34.7%

spectral-based wave modeling and ocean engineering applications. The simulation of PRTWs in this work is conducted to generate a segment containing 50 wave crests as wave energy input, with the time step of 0.001 s and wave speed of 6.0 m/s. The statistical distributions of wave height and period are generated using the Rayleigh and Gaussian distributions, following the methodology described in Ref. [47]. A sinusoidal speed within 1 ± 0.1 r/s is generated as tidal turbine input. The load resistance is 1.0 kΩ. The simulated input force, input torque, and output voltage are shown in Fig. 6. The average input power and output power are 402.8 W and 81.5 W, respectively, with the output voltage ranging from 230.2 V to 394.9 V. Compared to the minimum voltage of 117.7 V without overrunning, the introduction of the overrunning effect raised the minimum output voltage by 95.6% (Fig. 6b). This improvement is undoubtedly encouraging for powering PEM electrolyzers.

To match the capacity and structural strength of the prototype, the dimensions of the buoy and turbine are estimated. For a pontoon-type float, the static displacement should be at least 0.12 m^3 to generate sufficient driving force. To ensure response speed and robustness, the maximum draft depth should exceed 2 m. A conservative estimate gives a height of about 3 m and a cross-sectional diameter of 0.5 m. Assuming a tidal flow velocity of 1 m/s, a turbine radius of 0.2 m can meet the torque requirement of 5 N m. Thus, the energy density is 415.3 W/m^2, which is considerable at this scale, and larger prototypes will be necessary for practical applications.

4. PEM electrolyzer

4.1. PEM electrolyzer stack

The PEM electrolyzer stack adopted in this study prioritizes efficient catalysis, uniform current distribution, low impedance, and adaptability to the intermittent nature of wave and tidal energy, in order to ensure compatibility with varying energy availability in different offshore regions (Fig. 7).

Each unit cell consists of a proton exchange membrane (PEM), catalyst layer (CL), gas diffusion layer (GDL), and bipolar plate (BPP). The PEM is made of commercially mature Nafion series materials, offering high proton conductivity, low gas permeability, and excellent chemical stability. IrO_2 and RuO_2 are typically used as the anode catalyst, while Pt/C is employed as the cathode catalyst to enhance hydrogen evolution reaction (HER) performance. The bipolar plates are constructed from titanium-based coated materials or carbon-based materials to minimize corrosion and improve electrical conductivity. The parallel flow field is adopted for the bipolar plate channels design to optimize water management and enhance overall cell performance. Given the power fluctuations associated with the wave or tidal energy, an external water-cooling system is implemented in the PEM electrolyzer to maintain an optimal operating temperature within 60~80 °C. Additionally, a recirculating water system is utilized to sustain the membrane hydration, preventing the performance degradation caused by its dehydration.

4.2. Voltage modeling

The electrochemical reactions occurring at the interfaces between the bipolar plate and the anode and cathode electrodes in each PEM unit cell are the oxygen evolution reaction (OER) and the hydrogen evolution reaction (HER), respectively.

$$\text{Anode}: H_2O \rightarrow 0.5O_2 + 2H^+ + 2e^- \tag{8}$$

$$\text{Cathode}: 2H^+ + 2e^- \rightarrow H_2 \tag{9}$$

The operating voltage V of a single PEM unit cell is primarily influenced by various overpotentials.

$$V = V_{ocv} + V_{act} + V_{diff} + V_{ohm} \tag{10}$$

where V_{ocv} is the open circuit voltage, V_{act} is the activation voltage, V_{diff} is the diffusion overpotential caused by the mass transport, and V_{ohm} is the ohmic overpotential caused by the resistances.

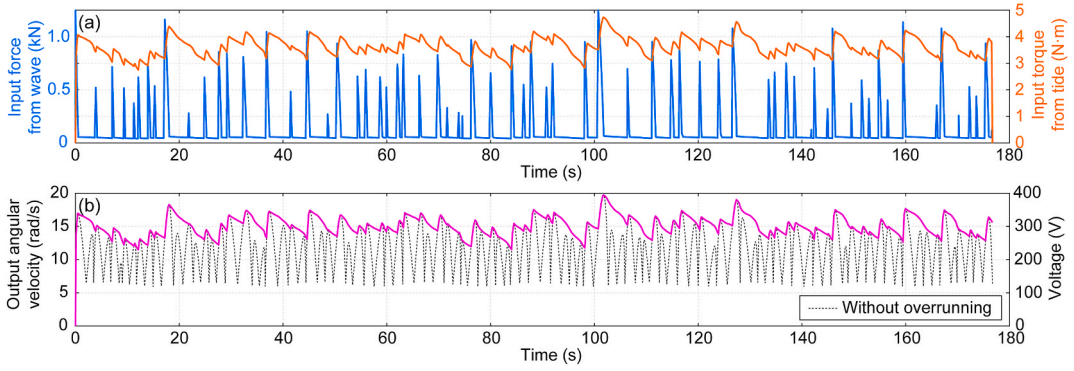

Fig. 6. Performance simulation with discrete pseudo real-time wave data.

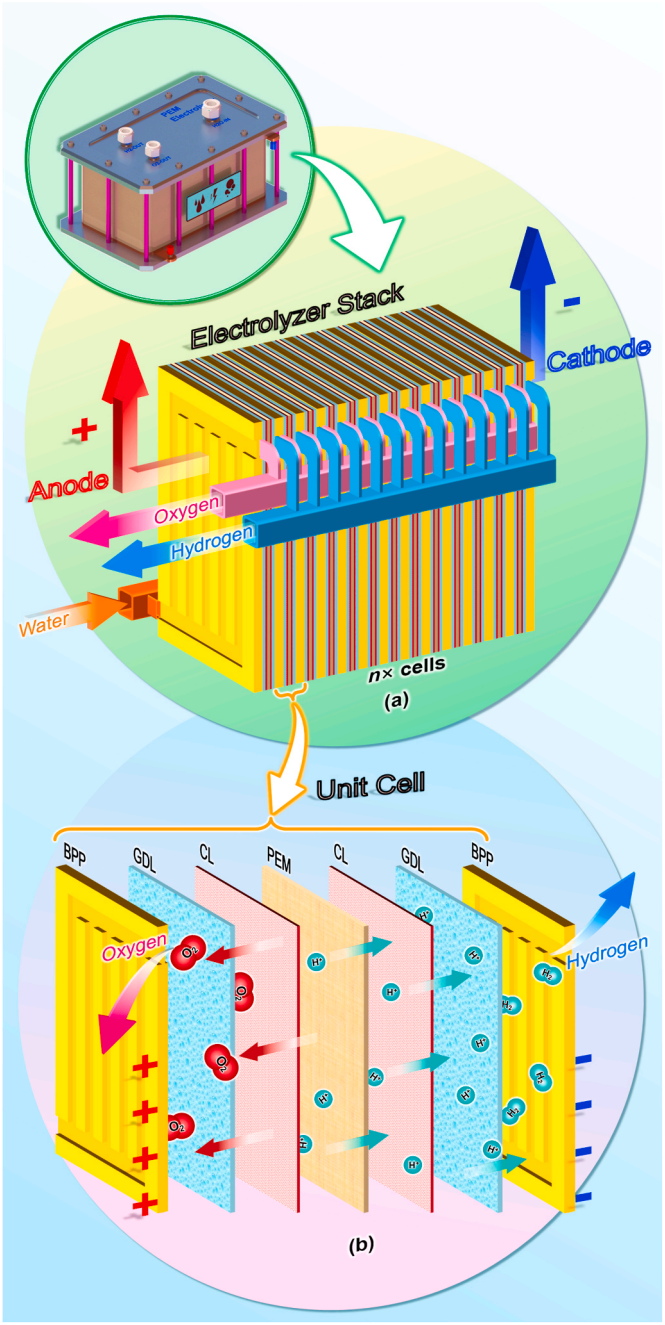

Fig. 7. PEM electrolyzer stack and unit cell.

The open-circuit voltage V_{ocv} defines the theoretical minimum voltage required to drive the electrochemical reactions in PEM electrolyzer cells under ideal and no-current conditions, neglecting other overpotentials.

$$V_{ocv} = \frac{\Delta G}{zF} + \frac{RT}{zF}\ln\left(\frac{\alpha_{H_2}\alpha_{O_2}^{0.5}}{\alpha_{H_2O}}\right) \tag{11}$$

where ΔG is the Gibbs free energy change in the reaction. R is the gas constant, which is 8.314 J/(mol·K). T is the electrolyzer operating temperature, usually in the range of 333.16–353.16 K. z is the mole number of electrons transferred in the electrolysis, which is 2 in this study. F is the Faraday constant, which is 96485.3 C/mol. The activity of species i, denoted as α_i, is defined as $\alpha_i = P_i/P_0$ for an ideal gas, where P_i represents the partial pressure of species i and P_0 corresponds to the standard atmospheric pressure. For liquid water, the activity α_{H_2O} is 1.0. The partial pressure of hydrogen and oxygen in this study are set as 3–35 MPa and 101 kPa, respectively.

The overall activation overpotential V_{act} is the sum of the activation overpotentials at the anode and cathode.

$$V_{act} = V_{act,a} + V_{act,c} \tag{12}$$

The OER at the anode is a four-electron process with relatively slow kinetics, typically resulting in a higher activation overpotential $V_{act,a}$. In contrast, the HER at the cathode proceeds with faster kinetics and a lower activation overpotential $V_{act,c}$, although it remains non-negligible. The activation overpotentials at the anode and cathode can be expressed using the Tafel equations as follows:

$$V_{act,a} = \frac{RT_a}{\alpha_a F}\sinh^{-1}\left(\frac{j}{2j_{0,a}}\right) = \frac{RT_a}{\alpha_a F}\ln\left(\frac{j}{2j_{0,a}} + \sqrt{1+\left(\frac{j}{2j_{0,a}}\right)^2}\right) \tag{13}$$

$$V_{act,c} = \frac{RT_c}{\alpha_c F}\sinh^{-1}\left(\frac{j}{2j_{0,c}}\right) = \frac{RT_c}{\alpha_c F}\ln\left(\frac{j}{2j_{0,c}} + \sqrt{1+\left(\frac{j}{2j_{0,c}}\right)^2}\right) \tag{14}$$

where T_a and T_c present the anode and cathode operating temperature respectively, which are regarded equal and equal to the operating temperature T. α_a and α_c are the charge transfer coefficients of the anode and cathode, which are 2.0 and 0.5 respectively in this study. The current density j is usually in the range of 0.1–3.0 A/cm^2. The $j_{0,a}$ and $j_{0,c}$ are the exchange current density on the anode and cathode, which vary greatly in different studies, ranging from 1.65×10^{-8}–2.00×10^{-6} A/cm^2 and 1.00×10^{-5}–1.00×10^{-1} A/cm^2, respectively [43]. In this study, values for a moderate operating condition are taken as 1.65×10^{-8} A/cm^2 and 9.0×10^{-2} A/cm^2, respectively.

The diffusion overpotential V_{diff} is caused by the mass transport, which can be expressed by an equation derived from the Nernst equation.

$$V_{diff} = \frac{RT_a}{4F}\ln\left(\frac{C_{O_2,s}}{C_{O_2,b}}\right) + \frac{RT_a}{2F}\ln\left(\frac{C_{H_2,s}}{C_{H_2,b}}\right) \tag{15}$$

where $C_{O_2,s}$ and $C_{H_2,s}$ are the oxygen and hydrogen concentrations on electrode surface, respectively, $C_{O_2,b}$ and $C_{H_2,b}$ are the bulk concentrations of oxygen and hydrogen. The ratios for oxygen and hydrogen are usually ranged in 2.0–5.0 and 1.0–2.0, respectively, determined by the reaction rate. If the gas is not discharged smoothly and accumulates, the ratio will be higher.

The ohmic overpotential V_{ohm} is caused by the resistances.

$$V_{ohm} = V_{ohm,a} + V_{ohm,c} + V_{ohm,m} = jA\cdot(R_a + R_c + R_m) \tag{16}$$

where $V_{ohm,a}$, $V_{ohm,c}$ and $V_{ohm,m}$ are the voltages of anode, cathode and membrane respectively, determined by their resistance R_a, R_c and R_m. A is the reaction area. The resistance values are selected according to literature [42,43]. Specifically, the membrane conductivity (unit: S/cm) is generally determined by the following empirical equation:

$$\sigma_m = (0.005139\lambda - 0.00326)\exp\left[1268\left(\frac{1}{303} - \frac{1}{T}\right)\right] \tag{17}$$

where, λ represents the membrane humidification degree, which ranges 14–25; a value of 20 is adopted in this study. At the current density of 1.0 A/cm^2, temperature of 353.16 K, and a membrane thickness of 178 μm, the membrane conductivity is 0.18 S/cm, corresponding to an ohmic overpotential of 0.099 V. Since the ohmic overpotential loss caused by the membrane resistance dominates the total ohmic overpotential, accounting for approximately 63.6% [43], the variation of total ohmic overpotential V_{ohm} with temperature can thus be obtained.

The simulated operating voltage V required for a single PEM unit cell under various current density conditions is presented in Fig. 8. As the temperature increases, the overall cell voltage decreases, primarily due

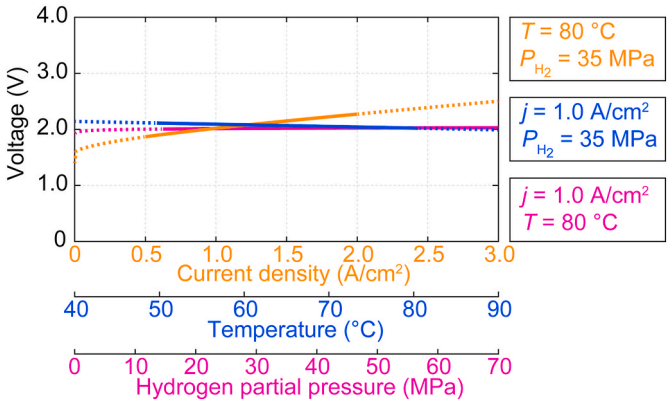

Fig. 8. Impact of key factors on the voltage behaviour in a PEM Electrolyzer unit cell.

to the reduction of the reversible voltage. Conversely, an increase in current density raises the required voltage. The rise in hydrogen partial pressure increases gas removal resistance, thereby requiring a higher voltage to sustain the electrolysis reaction. The cell voltage is relatively insensitive to variations in operating temperature and hydrogen partial pressure. Hence, the system integration can primarily focus on hydrogen storage efficiency. The cell voltage is more sensitive to changes in current density, necessitating a balance between electrolysis efficiency and thermal management. Considering the power fluctuation features of wave and tidal energy, a commonly used current density of 1.0 A/cm^2 under partial load operations is selected in this study to ensure hydrogen production efficiency, safety margins and system robustness. Under these conditions, the required voltage for a single cell is approximately 2.0 V. Given the wide variation in reported values of electrode exchange current density in the literature, a sensitivity analysis was conducted to examine its influence under the considered operating conditions. The results indicate that, at a nominal current density of 1.0 A/cm^2, variations in electrode exchange current density lead to a single-cell voltage range of 1.9–2.3 V, which is consistent with the results of 1.8–2.3 V reported in Ref. [43]. Such voltage variations induce only minor deviations in current density, which remain well within the stable operating window of the PEM electrolyser. Therefore, the power configuration designed based on a nominal cell voltage of 2.0 V provides sufficient operational margin to accommodate the entire voltage range without compromising stable operation.

5. System integration and case study

With considering the site selection and local energy availability, the integration of hybrid wave-tidal energy conversion systems with PEM electrolyzer stacks prioritizes dynamic power matching and system compatibility.

5.1. Site selection

By overlaying the wave energy distribution (Fig. 9a) and tidal energy distribution (Fig. 9b) around the UK, the potential deployment areas for HWTECs can be identified.

The wave and tidal resource datasets were obtained from the UK Renewable Energy Atlas [50] and processed into raster layers for spatial analysis in ArcGIS. These were combined to produce the integrated hybrid wave-tidal energy potential map (Fig. 9c). Offshore wind farm locations, depleted gas fields, and offshore pipeline routes were sourced from the North Sea Transition Authority Data Centre [51] and spatially overlaid on the combined energy map to highlight potential subsea storage opportunities (Fig. 9c). Building on this, a specific deployment area was identified (Fig. 9d) by considering both the energy resource

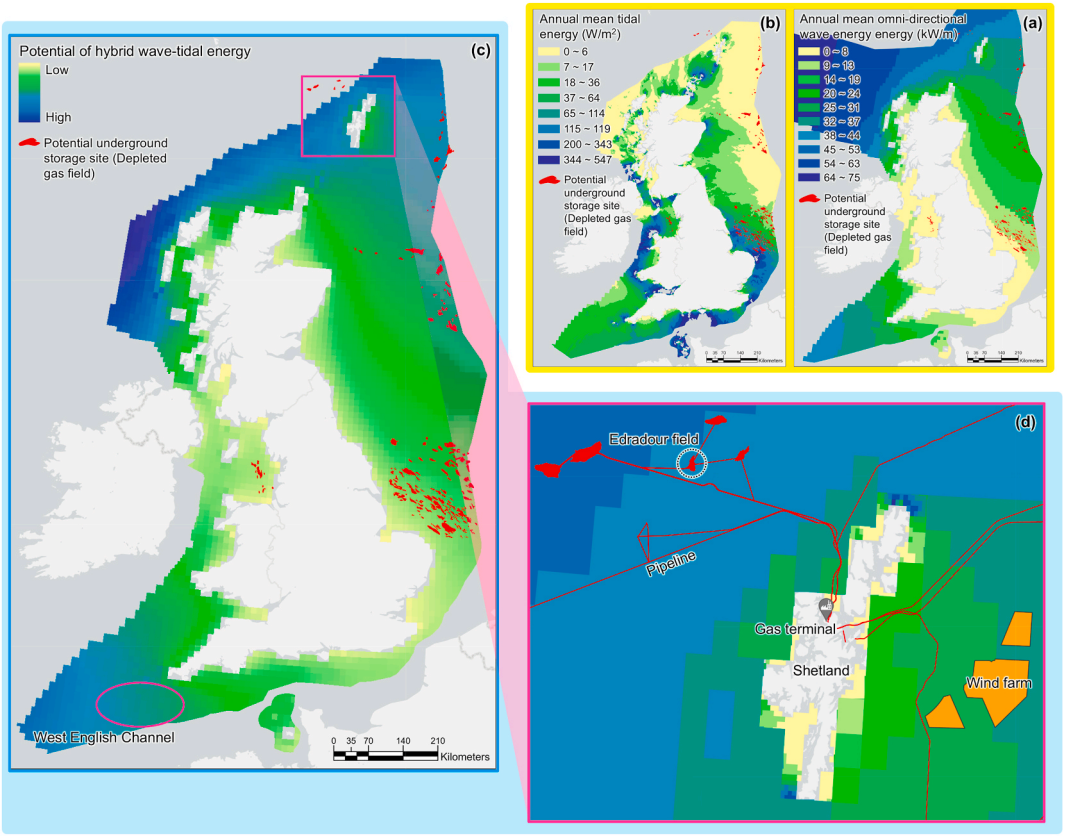

Fig. 9. Wave energy and tidal energy distribution and potential underground hydrogen storage sites around the UK.

distribution and infrastructure availability.

Moreover, the West English Channel was also selected as one case study area for offshore hydrogen production, due to its considerable levels of wave and tidal energy and the availability of extensive marine observation data. Its proximity to Atlantic shipping lanes also facilitates hydrogen transport, making high-pressure hydrogen vessels a feasible option for storage and delivery.

In addition to widely adopted pressure hydrogen vessels, underground hydrogen storage (UHS) represents a promising alternative, particularly for large-scale and long-duration storage. UHS stores hydrogen in subsurface geological formations, enabling injection during surplus production and withdrawal during demand peak. This approach provides inter-seasonal energy balancing and improves grid flexibility [52]. Additionally, the storage costs constitute a significant portion of the LCOH, while UHS is crucial for increasing production and reducing storage costs. Compared to the cost of approximately \$700–850/kgH_2 in stationary storage vessels [53], the average cost of UHS is no more than \$1.5/kgH_2 [54]. The UHS assessment also provides a fundamental basis that allows realistic evaluation of deployment sites, accounting for multiple hydrogen storage methods and avoiding misjudgement of industry feasibility. Among various geological options, depleted gas fields are considered highly suitable due to their proven capacity to safely retain pressurized gas over geological timescales. Hence, the connection between underground hydrogen storage (UHS) and offshore hydrogen production platform is an essential practical basis of the case study. Specifically, the large storage potential offered by UHS allows for the reduction or even omission of onboard hydrogen vessels when planning platform deployments, allowing more hydrogen production systems deployed. This directly decides the design of rated power, platform configuration and site selection in this paper.

A recent national assessment using Geographic Information System (GIS) screened 71 depleted gas fields in the UK based on reservoir quality, injectivity and deliverability, storage capacity, cushion gas requirements, and infrastructure accessibility [55]. Among the evaluated sites, the waters around the Shetland and Orkney Islands were identified as the most suitable region for integrated offshore hydrogen production and storage (Fig. 9c and d). The Edradour gas field located here, offers a promising combination of geological and infrastructural advantages. It features high-quality reservoir rock with average porosity of 17.5% and permeability of 340 mD, enabling excellent injectivity and deliverability, up to 2×10^8 sm^3/d. This supports an estimated working gas capacity of around 10 billion sm^3, equivalent to approximately 27 TWh of energy storage. Furthermore, the low cushion gas ratio (approximately 1:1) here significantly reduces initial gas injection requirements and associated costs. Its existing connection to the Sullom Voe gas terminal and offshore pipeline network further enhances its suitability by minimizing infrastructure development.

These two selected deployment regions can consider the assessment of both production potential and storage feasibility, laying the groundwork for future integrated offshore hydrogen systems.

In 2024 (Table 4), the monthly average significant wave height at the selected site ranges from 1.0 to 2.1 m, and the dominant wave period varies between 7.5 and 12.7 s [56]. The annual mean tidal stream speed exceeds 1.0 m/s [57]. To match current small-scale offshore platforms with the wave-facing width of approximately 20∼50 m, the diameter of individual WEC buoys is preferably no greater than 6 m. Compatible tidal turbines typically have an equivalent blade length of no more than 3 m. The power that each such HWTEC can output ranges from 6.9 to 25.1 kW (Table 4). Wave and tidal energy resources exhibit seasonal variability, with significantly higher power availability during spring and winter compared to summer and autumn.

However, due to the occasional occurrence of extreme sea conditions in spring and winter, wave and tidal energy in a portion of high-energy scenarios cannot be captured for safety reasons. Consequently, the useable energy exceeding the rated capacity of the electrolyzers is not as abundant as the data might suggest. Hence, the installed capacity of the electrolyzer system can be appropriately reduced to ensure efficiency and save budget.

5.2. Power matching

To ensure consistent power matching across different scales, the full-scale HWTEC is designed to simulate real marine deployment. It is important to notice that, the scaling between application-scale device and laboratory-scale prototype is functional, rather than proportional. Dimensions of the full-scale system are determined based on the strength and power demands (Fig. 10 and Table 4) of key components such as shafts, gears, bearings, and generators, rather than proportional scaling. Such functional sizing and verification methods are widely used in wave or tidal energy conversion studies [7,22], regarded sufficient at this stage to ensure consistent power matching across different scales. More detailed scale considerations and standardization will be addressed in future development stages. According to the scale of offshore platforms and HWTEC dimensions mentioned above, this study proposes deploying a 2×3 array of full-scale HWTECs aligned with the wave propagation direction, with each buoy diameter of 6 m and turbine blades equivalent length of 3 m. To minimize hydrodynamic interference, the devices are spaced >60 m apart in tidal streamwise direction and >20 m apart laterally. Under the daily ocean conditions simulated in Section 3.3, a time-domain simulation lasting 420 s (Fig. 10) is conducted to assess the input conditions and output performance of each full-scale HWTEC.

The peak input forces and input torque from waves and tides reach 146.5 kN and 2.16 kN m, respectively, with average input powers contributing 26.1 kW and 10.2 kW (Fig. 10b). The peak output voltage reached 375.2 V (Fig. 10c), and the average output power is 10.8 kW. The total average power generated by 6 sets of full-scale HWTECs reaches 64.8 kW, with rated power of 108.0 kW.

Reported offshore platform applications indicate that the typical average power demand for daily operations generally ranges 20–50 kW, such as the multi-purpose platforms in Ref. [58]. Compared to the electricity cost required for PEM electrolyzer operation, the cost of producing water of necessary quality for the electrolyzer is significantly lower, resulting in a minimal impact on the overall hydrogen production cost, accounting for less than 2% [59,60]. The power consumption of pumps and compressors covers 1%∼4% [60]. Considering the PEM electrolyzer capacity factor of 70∼90% for optimal economics [61] and power margin about 20%, the rated power of the PEM electrolyzers is set approximately 78.0 kW (capacity factor of 72.2%) to balance the efficiency and cost. This capacity is well matched to the local wave and tidal energy potential, supporting operation near full load for most of the time while maintaining safety margin.

With a current density of 1.0 A/cm^2 and a single cell voltage of 2.0 V,

Table 4
Input parameters and output power of HWTEC based on 2024 data.

Month	Wave energy input		Tidal energy input	Total
	Significant Wave Height (m)	Dominant Wave Period (s)	Stream speed (m/s)	Average output power (kW)
Jan.	1.9	12.4	1.0	20.7
Feb.	2.1	12.7	1.0	25.1
Mar.	1.8	11.6	1.0	18.4
Apr.	1.6	9.1	1.0	11.9
May.	1.0	9.0	1.0	6.9
Jun.	1.2	7.5	1.0	7.4
Jul.	1.1	8.0	1.0	6.9
Aug.	1.5	9.5	1.0	11.3
Sep.	1.2	8.5	1.0	8.3
Oct.	1.5	11.4	1.0	12.7
Nov.	1.2	10.5	1.0	9.5
Dec.	2.1	10.7	1.0	21.1

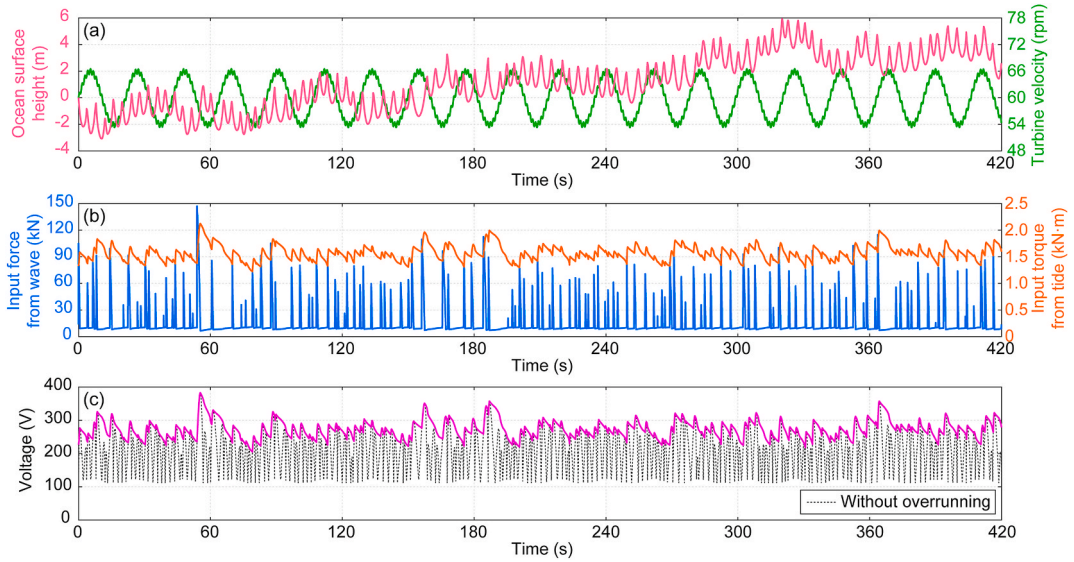

Fig. 10. Simulation of single full-scale HWTEC in pseudo real-time wave conditions.

the total active membrane area required is 39,000 cm^2. Using commercially available PEM units with an individual active area of 250 cm^2, a total of 156 cells is required. To alleviate thermal management pressure, the system is divided into three PEM stacks, each comprising 52 cells. The volume of each PEM stack can be kept below 200 L.

The supercapacitor module is allowed to charge to the rated voltage within a few minutes during system startup. Once fully charged, it is connected to the PEM electrolyzer, serving as temporary energy storage and voltage buffer. Its charge/discharge and energy storage capacity are as follows:

$$E_s = \frac{1}{2} C\left(V_{high}^2 - V_{low}^2\right) \tag{18}$$

where E_s is the energy stored or released, C is the capacitance, V_{high} and V_{low} are the initial and final voltages during charging or discharging, respectively. This study proposes to use 6 supercapacitor modules, each with rated voltage of 104 V to buffer voltage fluctuations for the PEM electrolyzer, maintaining voltage above 80% of the rated value for at least 20 s and above 5% for up to 5 min, thus reducing shutdown and restart events. Based on Eq. (18), each supercapacitor module requires the capacitance of 600.6 F and energy capacity of 0.9 kW h. At an average input power of 10.8 kW, it can be charged to the rated voltage within around 5 min, and reach the minimum startup voltage (5% of rated) of the PEM electrolyzer within a few seconds. Referencing commercially available supercapacitor cells, each complete supercapacitor module, including cooling, is estimated to remain under 300 L in volume, making integration technically feasible. Considering that peak power in high-energy seasons may exceed the average by several times, dynamic allocation of HWTEC units is recommended to balance input and prevent overload. Under extreme conditions, active disconnection strategies may be employed to protect system components.

In terms of compatibility, most generators used in renewable energy systems are alternating current (AC) generators, as they help reduce maintenance costs and improve efficiency. However, both PEM electrolyzers and the supercapacitors introduced for temporary energy storage and voltage buffering require direct current (DC) power. Therefore, rectifiers are essential to convert the AC output into DC power. Additionally, the installed capacity of the HWTEC, the storage capacity of the supercapacitor, and the rated power of the PEM electrolyzer must be coordinated according to the offshore platform scenario, to ensure the energy capture and conversion efficiency of ocean energies.

5.3. System co-simulation

Based on the dynamic model of the HWTEC, the electrochemical model of the PEM electrolyzer, and their power matching, a co-simulation framework is established in Matlab and Simulink to provide the common simulation environment, unified data format, and seamless interoperability. In this framework, the HWTEC output calculated by the sub-module in Ref. [47] can input the ESS, and then power the PEM electrolyzer. The battery-electrolyzer coordination strategy controls the energy distribution based on the battery parameters (Table 5) and output power of HWTEC. Specifically, electrolyzers start when HWTEC output power buffered by the supercapacitor exceeds 10% of rated power; extra power above rated power of electrolyzers charges the battery up to its maximum depth. The battery discharges to support the electrolyzer when HWTEC power drops below rated and state-of-charge exceeds 40%, while charging and discharging are limited by predefined depth thresholds to avoid frequent cycling. The above process enables direct data transmission and co-simulation of the integrated system to determine the hydrogen production rate. The hydrogen production rate is,

$$\dot{m}_{H_2} = \frac{\dot{I} M_{H_2}}{2F} \cdot \eta_f \tag{19}$$

where, $\dot{m}_{H_2}$ is the mass of hydrogen generated per unit time, $\dot{I}$ is the instantaneous current, M_{H_2} is the molar mass of hydrogen, η_f is the Faradaic efficiency, which is 96% in this study [62].

The voltage and hydrogen production rate of the PEM electrolyzer are simulated as Fig. 11. To ensure a stable voltage supply, HWTECs are connected to the system initially to charge the supercapacitor modules, while the PEM electrolyzers remain offline (Fig. 11a). The supercapacitors reach the rated voltage within 300 s (Fig. 11b), after which the PEM electrolyzer is connected, causing a slight voltage drop. During the stable operating period from 300 s to 600 s, the HWTECs maintain the electrolyzers voltage close to the nominal level, enabling efficient operation in the optimal range. The hydrogen production rate ranges from 1226.6 to 1417.3 g/h, yielding total output of 544.4 g over 10 min (Fig. 11c). To simulate simultaneous wave and tidal pauses, HWTECs are disconnected at 600 s. The supercapacitors sustain the electrolyzer voltage above 80% of the nominal value for 86 s (Fig. 11b), exceeding a typical wave period. This indicates that the integrated system can maintain a hydrogen production rate above 1081.7 g/h under typical short-term fluctuations in wave and tidal energy.

Table 5
Parameters of the battery in co-simulation.

Rated voltage	320V (300~350V)	Useable capacity	20 kW h
Round-trip efficiency	95%	Max charge power	8 kW (0.4 C)
Depth of discharge	90%	Max discharge power	10 kW (0.5 C)

Additionally, to absorb excess power under high-energy conditions, a lithium battery with useable capacity of >20 kW h (nominal capacity of 24 kW h) and backup hydrogen storage vessels are recommended for each HWTEC, forming a hybrid energy storage system. In this configuration, the supercapacitor manages transient power fluctuations, while the lithium battery provides average power compensation. Simulation results show that when the output power of each HWTEC fluctuates around 20 kW, the lithium battery can be fully charged in at least 3 h while simultaneously supporting PEM electrolyzers. Under low-energy conditions of approximately 3 kW, it can sustain the continuous PEM electrolyzer operation, with full-load for about 2 h or with 60% rated power for about 4 h. This setup improves energy utilization, supports auxiliary demands such as hydrogen processing and compression, and helps offset production shortfalls during low-energy periods.

5.4. Configuration and deployment

It should be emphasized that the configuration of the small-scale offshore platform presented here is intended as a representative case. In practical deployment, multiple such platforms would be installed as a cluster, enabling the overall production capacity to be increased as required. This clustered approach allows the scaling of hydrogen output without increasing individual platform complexity, while fully exploiting the storage potential of the selected subsurface sites.

According to the power demand mentioned previously, a partial load of 40 kW can be assumed as a representative scenario. Approximately 173.0 kg of hydrogen is required to sustain 72 h of energy supply, considering the efficiency of 50% based on the lower heating value (LHV) of hydrogen.

In summary, the deployment configuration of the integrated hybrid wave-tidal energy powered PEM electrolyzer system for small-scale offshore platforms can be summarized as Fig. 12. Regarding space requirements, the fresh water storage needed to support one week of continuous operation of the 40 kW PEM electrolyzer is estimated at 2.3 m^3, accounting for engineering factors such as circulation losses and safety margins. The volumes required for the PEM electrolyzer stack and battery system are approximately 200 L and 300 L, respectively. Considering additional auxiliary equipment and assuming a platform occupancy factor of 50%, the total effective space required for the complete system can be maintained below 8.4 m^3. For comparison, if the hydrogen produced were to be stored entirely onboard using 35 MPa high-pressure storage vessels with quarterly offloading and a storage efficiency of 70%, the required space would increase dramatically by 146.4 m^3 per season. This represents an 18.4-fold increase compared to the use of UHS. Such a large space requirement would significantly encroach on available platform deck area, resulting in a substantial reduction in hydrogen production capacity for a given platform footprint and a marked increase in the LCOH. This highlights the key advantage of UHS in offshore hydrogen production, enabling compact platform layouts while maintaining high production capacity.

The spatial layout of the offshore platform and HWTECs is illustrated in Fig. 13a. For above integrated system, the monthly hydrogen production rate in 2024, calculated by using the wave and tidal parameters in Table 4 together with the output performance of the integrated system, is illustrated in Fig. 13b, with an estimated annual yield of 12.4 t. Under non-extreme sea conditions, the system with rated hydrogen production of 2.0 kg/h can operate at over 70% capacity mostly during spring and winter, while simultaneously supplying surplus electricity for additional onboard demands such as heating. In this scenario, the hydrogen production energy consumption (LHV) ranges from 46.8 to 55.7 kW h/kgH_2. In summer, although resource availability decreases, the system can still meet typical power demand of approximately 40 kW on platform. Even in July, the lowest production month, the system can startup when the input power reaches the minimum operation power (~5% of rated power) produce 608.0 kg of hydrogen, sufficient to power the platform for approximately 10.5 days. Even under extremely low-energy conditions, where the input power falls below 5% of the PEM electrolyzers rated capacity, the temporary energy storage system composed of the battery and supercapacitor can still store and accumulate the captured energy. Once the discharge conditions are met, it continues to supply power to the PEM electrolyzer, thereby enabling full utilization of all the available energy during low-energy periods. Considering the HWTEC efficiency of 29.8% and the average efficiency of PEM electrolyzers of 69.4%, the overall efficiency of the integrated system is estimated to be 18.5%~21.6%. Compared with similar hybrid

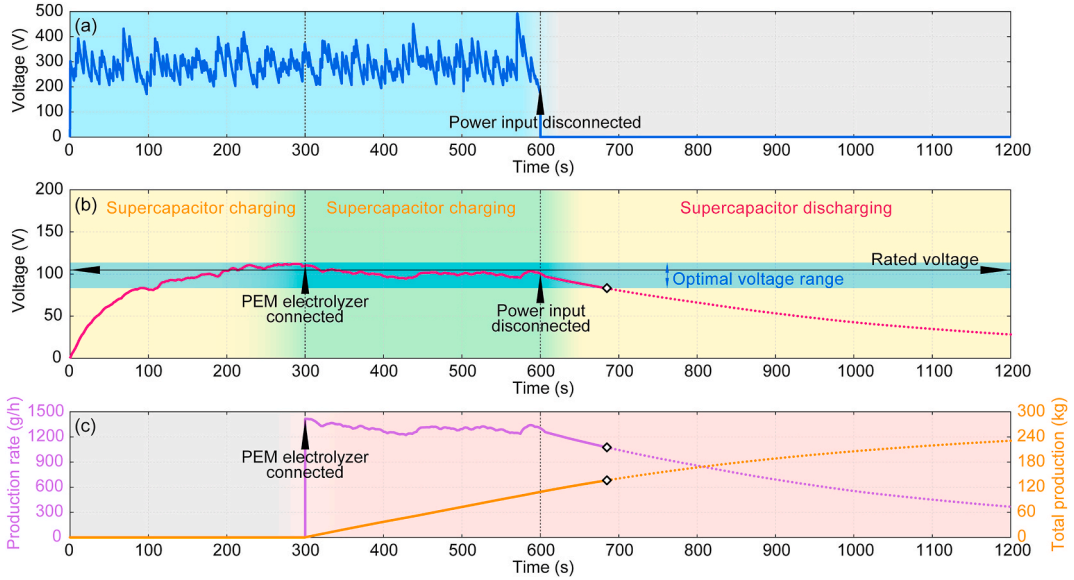

Fig. 11. Simulation of supercapacitor voltage and hydrogen production.

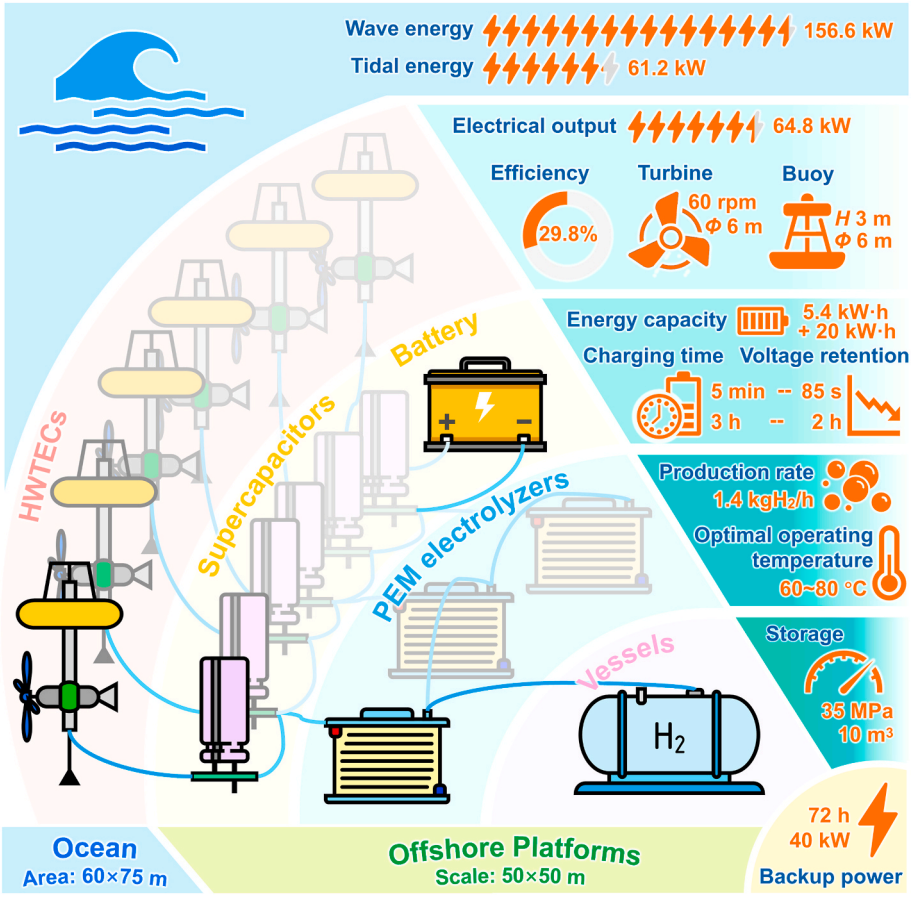

Fig. 12. Integration configurations of the hybrid wave-tidal energy powered PEM electrolyzer system.

systems reported in previous studies, which achieved efficiencies of 15.4% [15,30]0.83% [32], and 25.64% [27], the proposed hybrid wave-tidal energy hydrogen production system demonstrates a competitive overall efficiency. These results demonstrate that, with proper energy management strategies, it is feasible to maintain a net-positive hydrogen reserve on such small-scale offshore platforms under comparable resource conditions.

For offshore platforms deployed around the Shetland Islands, higher available wave and tidal energy allows for greater deployment capacity and scale of HWTECs. When integrated with the nearby offshore wind farms, hydrogen production can be further enhanced significantly, enabling the use of existing pipeline infrastructure to inject hydrogen into surrounding underground storage formations.

6. Conclusion

This study develops an integrated offshore hydrogen production system coupling a hybrid wave-tidal energy converter (HWTEC) with a proton exchange membrane (PEM) electrolyzer, establishing a co-simulation framework for end-to-end analysis from ocean energy inputs to hydrogen output. The main contributions and findings are summarized as follows:

(a) System-level integration and modeling

A full-scale HWTEC was designed and included as a sub-module, which enables direct use of real stochastic wave and tidal data and provides discretized nonlinear power inputs for subsequent sub-modules.

A unified co-simulation framework couples HWTEC, battery storage, PEM electrolyzer, and hydrogen storage, allowing coordinated evaluation of energy conversion, buffering, and hydrogen production under realistic offshore conditions.

(b) Simulation validation and performance assessment

Based on measured wave and tidal data from the English Channel, a conceptual offshore platform with six HWTEC units achieved average output of 64.8 kW and an estimated annual hydrogen yield of 12.4 t, with specific energy consumption of 46.8–55.7 kWh/kgH_2 and exergy efficiency of 21.4–25.3%.

(c) Enhanced operational continuity and storage utilization

Coupling wave and tidal energy with battery buffering mitigates intermittency, providing a controllable power input to the electrolyzer. This enables the conversion of intermittent offshore renewable electricity into storable and transportable hydrogen.

The framework incorporates subsea underground hydrogen storage (UHS), which reduces the required platform storage volume by a factor of 18.4 compared to conventional high-pressure vessels, thereby enabling higher hydrogen production capacity, and also facilitating cost-effective hydrogen distribution for large-scale deployment.

In summary, this study presents a system-level framework integrating hybrid wave-tidal energy, battery energy storage, PEM electrolysis, and subsea underground hydrogen storage, directly incorporating real offshore conditions. The framework enables coordinated assessment of energy conversion, storage efficiency, and hydrogen production under stochastic marine environments, providing a scalable and practical tool for the design and optimization of offshore hybrid

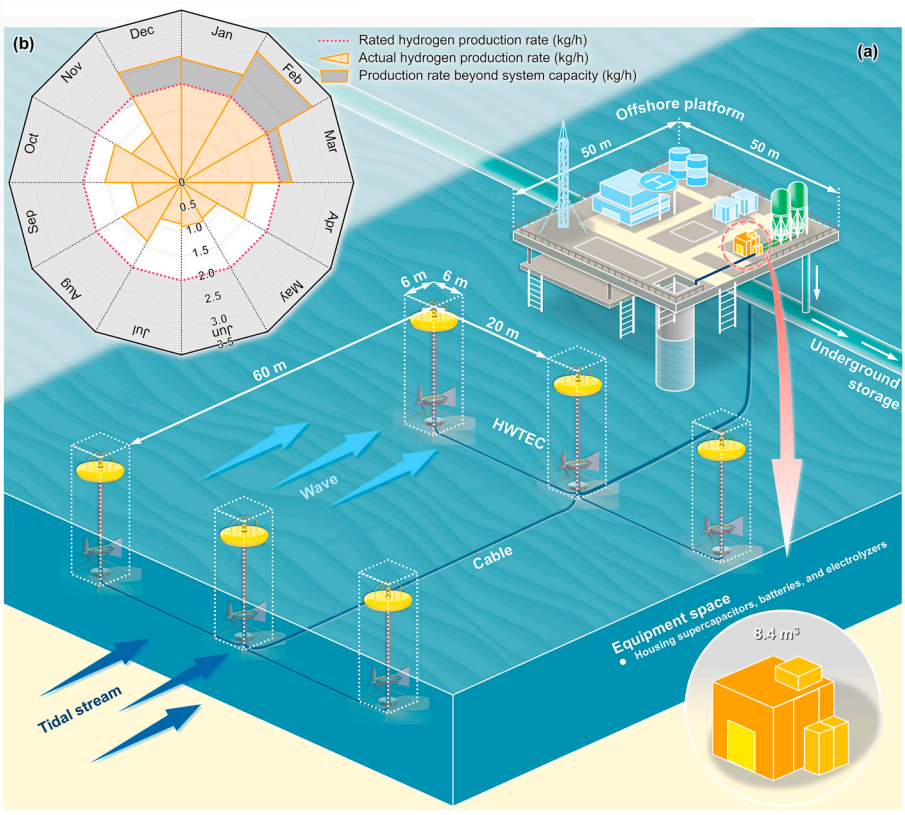

Fig. 13. Spatial layout of the offshore platform and HWTECs, with simulated monthly hydrogen production rate based on 2024 data.

renewable hydrogen platforms. Despite its advances, limitations remain, including seasonal variability of wave and tidal resources, the simplified dynamic representation of the PEM electrolyzer, and the absence of detailed techno-economic evaluation. Future work will extend the framework to incorporate comprehensive economic analysis and refined underground hydrogen storage assessments to evaluate commercial viability for large-scale deployment.

CRediT authorship contribution statement

Peihao Chen: Writing – review & editing, Writing – original draft, Visualization, Validation, Software, Methodology, Investigation, Formal analysis, Data curation, Conceptualization. **Yan Zhang:** Writing – review & editing, Visualization, Software. **Saeed Harati:** Writing – original draft, Visualization, Data curation. **Sara Walker:** Resources, Project administration, Funding acquisition. **Karl Dearn:** Supervision, Resources, Project administration, Formal analysis.

Declaration of competing interest

The authors declare that they have no known competing financial interests or personal relationships that could have appeared to influence the work reported in this paper.

Acknowledgements

The authors are thankful for the financial support from the EPSRC (the Engineering and Physical Sciences Research Council) of the United Kingdom via the research project EP/X038823/2.

Data availability

Data will be made available on request.

References

[1] Liu J, Ma X, Lu C. A three-stage framework for optimal site selection of hybrid offshore wind-photovoltaic-wave-hydrogen energy system: a case study of China. Energy 2024;313:133723. https://doi.org/10.1016/j.energy.2024.133723.
[2] Chen P, Wu D. A review of hybrid wave-tidal energy conversion technology. Ocean Eng 2024;303:117684. https://doi.org/10.1016/j.oceaneng.2024.117684.
[3] Jariwala AM, Dash SK, Sahu UK, Mohan HM. Performance optimization techniques on point absorber and oscillating water column wave energy converter: a comprehensive review. IEEE Access 2025;13:14743–59. https://doi.org/10.1109/ACCESS.2025.3531298.
[4] Hu H, Xue W, Jiang P, Li Y. Bibliometric analysis for ocean renewable energy: an comprehensive review for hotspots, frontiers, and emerging trends. Renew Sustain Energy Rev 2022;167:112739. https://doi.org/10.1016/j.rser.2022.112739.
[5] Yin X, Zhao X, Zhang W. A novel hydro-kite like energy converter for harnessing both ocean wave and current energy. Energy 2018;158:1204–12. https://doi.org/10.1016/j.energy.2018.03.121.
[6] Silva RN, Nunes MM, Oliveira FL, Oliveira TF, Brasil ACP, Pinto MSS. Dynamical analysis of a novel hybrid oceanic tidal-wave energy converter system. Energy 2023;263:125933. https://doi.org/10.1016/j.energy.2022.125933.
[7] Calheiros-Cabral T, Clemente D, Rosa-Santos P, Taveira-Pinto F, Ramos V, Morais Y, et al. Evaluation of the annual electricity production of a hybrid breakwater-integrated wave energy converter. Energy 2020;213:118845. https://doi.org/10.1016/j.energy.2020.118845.
[8] Jiang B, Li X, Chen S, Xiong Q, Chen B-f, Parker RG, et al. Performance analysis and tank test validation of a hybrid ocean wave-current energy converter with a single power takeoff. Energy Conv Manag 2020;224:113268. https://doi.org/10.1016/j.enconman.2020.113268.
[9] Chen S, Jiang B, Li X, Huang J, Wu X, Xiong Q, et al. Design, dynamic modeling and wave basin verification of a hybrid wave-current energy converter. Appl Energy 2022;321:119320. https://doi.org/10.1016/j.apenergy.2022.119320.
[10] Park M-S, Lee S-H, Ko S-C. Experimental capture width ratio on unit module system of hybrid wave energy converter for nearshore. Appl Sci 2022;12(12):5845. https://doi.org/10.3390/app12125845.
[11] Cheng Y, Dai S, Dai S, Ji C, Collu M, Yuan Z, et al. Energy conversion and hydrodynamic analysis of multi-degree-of-freedom wave energy converters integrated into a semi-submersible platform. Energy Conv Manag 2022;252:115075. https://doi.org/10.1016/j.enconman.2021.115075.
[12] Fang H, Wei Y, Feng Y. Investigation of a double-degree-of-freedom wave energy converter. Energy Rep 2020;6:402–6. https://doi.org/10.1016/j.egyr.2020.11.223.

[13] Gao H, Yu Y. The dynamics and power absorption of cone-cylinder wave energy converters with three degree of freedom in irregular waves. Energy 2018;143:833–45. https://doi.org/10.1016/j.energy.2017.11.036.
[14] Zou C, Li J, Zhang X, Jin X, Xiong B, Yu H, et al. Industrial status, technological progress, challenges, and prospects of hydrogen energy. Nat Gas Ind B 2022;9(5):427–47. https://doi.org/10.1016/j.ngib.2022.04.006.
[15] Pegler DL, Greaves D, Rawlinson-Smith R, Michele S, Conley D, Benhin J. Techno-economic analysis for floating offshore wind and offshore green hydrogen. Int J Hydrogen Energy 2025;103:538–55. https://doi.org/10.1016/j.ijhydene.2025.01.172.
[16] Kheirani S, Houmani A, Jahangir MH. Economical investigation of green hydrogen supply for hydrogen-powered ship by off-grid wave and wind energy hubs. Energy Convers Manag X 2025;26:101006. https://doi.org/10.1016/j.ecmx.2025.101006.
[17] Yu B, Fan G, Sun K, Chen J, Sun B, Tian P. Adaptive energy optimization strategy of island renewable power-to-hydrogen system with hybrid electrolyzers structure. Energy 2024;301:131508. https://doi.org/10.1016/j.energy.2024.131508.
[18] Pompodakis EE, Orfanoudakis GI, Katsigiannis YA, Karapidakis ES. Hydrogen production from wave power farms to refuel hydrogen-powered ships in the Mediterranean Sea. Hydrogen 2024;5(3):494–518. https://doi.org/10.3390/hydrogen5030028.
[19] Taroual K, Nachtane M, Adeli K, Boulzehar A, Saifaoui D, Faik A. Marine renewable energy for hydrogen production: advancing towards a sustainable future through technological, economic, and environmental frontiers – a review. Renew Sustain Energy Rev 2026;226(B):116304. https://doi.org/10.1016/j.rser.2025.116304.
[20] Oni BA, Sanni SE, Misiani AN. Green hydrogen production in offshore environments: a comprehensive review, current challenges, economics and future-prospects. Int J Hydrogen Energy 2025;125:277–309. https://doi.org/10.1016/j.ijhydene.2025.03.429.
[21] Akdağ O. A new framework to green hydrogen production from ocean/sea renewable energy sources: a case study of the Türkiye. Appl Energy 2025;396:126247. https://doi.org/10.1016/j.apenergy.2025.126247.
[22] Macingwane Z, Schönborn A. Techno-economic analysis of green hydrogen production as maritime fuel from wave energy. Energies 2024;17(18):4683. https://doi.org/10.3390/en17184683.
[23] Kostidi E, Kotrikla AM, Maglara A, Lilas T. Sustainable fuel supply for very small island transportation: the potential of hybrid renewable energy and green hydrogen. J Mar Sci Eng 2025;13(3):579. https://doi.org/10.3390/jmse13030579.
[24] Rodríguez Castillo CA, Collu M, Brennan F. Design considerations and preliminary hydrodynamic analysis of an offshore decentralised floating wind-hydrogen system. Int J Hydrogen Energy 2024;89:496–506. https://doi.org/10.1016/j.ijhydene.2024.09.340.
[25] Sánchez-Dirzo R, González-Huerta RG, Mendoza E, Silva R, Sandoval-Pineda JM. From wave to jet and from jet to hydrogen: a promising hybrid system. Int J Hydrogen Energy 2014;39(29):16628–36. https://doi.org/10.1016/j.ijhydene.2014.03.134.
[26] Molina-Salas A, Perez-Romero JM, Santamaria M, Clavero M, Moñino A. Exergy assessment of hydrogen production by oscillating water column wave energy converter. Int J Hydrogen Energy 2025;157:150130. https://doi.org/10.1016/j.ijhydene.2025.150130.
[27] Kenez MC, Dincer I. Development and assessment of an offshore-based integrated hydrogen production and liquefaction system. Appl Therm Eng 2024;236(D):121574. https://doi.org/10.1016/j.applthermaleng.2023.121574.
[28] Mehrenjani JR, Gharehghani A, Nasrabadi AM, Moghimi M. Design, modeling and optimization of a renewable-based system for power generation and hydrogen production. Int J Hydrogen Energy 2022;47(31):14225–42. https://doi.org/10.1016/j.ijhydene.2022.02.148.
[29] Bekçi E, Koca K, Bashir MF. Design analysis of a wave energy converter for hydrogen generation near shoreline of Black Sea. Process Saf Environ Prot 2024;186:1–9. https://doi.org/10.1016/j.psep.2024.03.080.
[30] Kurniawan AT, Budiarto R, Prasetyo RB, Budiman A. Selecting an ideal site for oscillating-water-column (OWC) wave energy converter for hydrogen production in the Southern Coast of Yogyakarta, Indonesia. In: 2020 1st international conference on information technology, advanced mechanical and electrical engineering (ICITAMEE); 2020. p. 35–40. https://doi.org/10.1109/ICITAMEE50454.2020.9398402. Yogyakarta, Indonesia, October 13-14. IEEE.
[31] Ozturk M, Dincer I. System development and assessment for green hydrogen generation and blending with natural gas. Energy 2022;261(B):125233. https://doi.org/10.1016/j.energy.2022.125233.
[32] Gursoy M, Dincer I. Development of a solar-ocean based integrated plant with a new hydrogen generation system. Renew Energy 2024;235:121354. https://doi.org/10.1016/j.renene.2024.121354.
[33] Meharban F, Tang X, Yang S, Wu X, Lin C, Tan L, et al. Harnessing direct seawater electrolysis for a sustainable offshore hydrogen future: a critical review and perspective. Appl Energy 2025;384:125468. https://doi.org/10.1016/j.apenergy.2025.125468.
[34] Pham TD, Dinh VN, Trinh LC, Judge F, Leahy P. Dynamic assessment of decentralized hydrogen production and storage on a semi-submersible floating wind turbine platform. Int J Hydrogen Energy 2025;164:150832. https://doi.org/10.1016/j.ijhydene.2025.150832.
[35] Ning M, Yao Y, Zhan Y, Pan F, Fu Y, Chen D, et al. Hydrogen production from marine renewable energy: a review. Energies 2025;18(24):6490. https://doi.org/10.3390/en18246490.
[36] Pan Q, Wang B, Zhang L, Li Z, Yang Z. Whisk-inspired motion converter for ocean wave energy harvesting. IEEE ASME Trans Mechatron 2022;27(3):1808–11. https://doi.org/10.1109/TMECH.2021.3093939.
[37] Yang Y, Chen P, Liu Q. A wave energy harvester based on coaxial mechanical motion rectifier and variable inertia flywheel. Appl Energy 2021;302:117528. https://doi.org/10.1016/j.apenergy.2021.117528.
[38] Lu H, Wang X, Bai Z, Jia N, Xia H. FVCOM-CFD model-based study of hydraulic turbine arrays in Mount Putuo tidal current energy test site. Ocean Eng 2024;312(1):119079. https://doi.org/10.1016/j.oceaneng.2024.119079.
[39] Xu T, Haas KA, Gunawan B. Estimating annual energy production from short tidal current records. Renew Energy 2023;207:105–15. https://doi.org/10.1016/j.renene.2023.02.107.
[40] Chen P, Yang Y. Design, dynamics modeling, and experiments of a vibration energy harvester on bicycle. IEEE ASME Trans Mechatron 2023;28(5):2670–8. https://doi.org/10.1109/TMECH.2023.3246516.
[41] Wang X, Xia H, Guo Y, Duan Y, Wang M, Liu Y, et al. Research on field testing and assessment technology of ocean energy converters. Ocean Eng 2023;285(2):115539. https://doi.org/10.1016/j.oceaneng.2023.115539.
[42] Carmo M, Fritz DL, Mergel J, Stolten D. A comprehensive review on PEM water electrolysis. Int J Hydrogen Energy 2013;38(12):4901–34. https://doi.org/10.1016/j.ijhydene.2013.01.151.
[43] Han B, Steen SM, Mo J, Zhang F-Y. Electrochemical performance modeling of a proton exchange membrane electrolyzer cell for hydrogen energy. Int J Hydrogen Energy 2015;40(22):7006–16. https://doi.org/10.1016/j.ijhydene.2015.03.164.
[44] Yavuz H. Modelling and simulation of a heaving wave energy converter based PEM hydrogen generation and storage system. Int J Hydrogen Energy 2020;45(50):26413–25. https://doi.org/10.1016/j.ijhydene.2020.06.099.
[45] Taroual K, Nachtane M, Adeli K, Faik A, Boulzehar A, Saifaoui D, et al. Hybrid marine energy and AI-driven optimization for hydrogen production in coastal regions. Int J Hydrogen Energy 2025;118:80–92. https://doi.org/10.1016/j.ijhydene.2025.03.091.
[46] He X, Yang S, Zhou R, Chen K, Liu Z, Yue Z. Research on gear life reliability analysis based on accelerated life test. Mater Sci Eng Technol 2024;55(6):839–50. https://doi.org/10.1002/mawe.202300196.
[47] Chen P, Wu D, Yang Y, Tsolakis A. Discretization modeling with pseudo real-time waves input of the hybrid wave-tidal energy converter based on non-linear motions rectification and coupling device. Energy 2025;323:135615. https://doi.org/10.1016/j.energy.2025.135615.
[48] Li Z, Wang H. Ocean wave simulation based on wind field. PLoS One 2016;11(1):e0147123. https://doi.org/10.1371/journal.pone.0147123.
[49] Chen P, Wu D, Yang Y, Zhang Y, Tsolakis A, Dearn K. Development, dynamic analysis, and experimental evaluation of a hybrid wave-tidal energy converter featuring nonlinear dual inputs. Energy 2025;338:138880. https://doi.org/10.1016/j.energy.2025.138880.
[50] Atlas of UK Marine Renewable Energy Resources. ABPmer. https://www.renewables-atlas.info. [Accessed 1 June 2025].
[51] North Sea transition authority data centre. https://www.nstauthority.co.uk/data-and-insights. [Accessed 1 June 2025].
[52] Harati S, Gomari SR, Gasanzade F, Bauer S, Pak T, Orr C. Underground hydrogen storage to balance seasonal variations in energy demand: impact of well configuration on storage performance in deep saline aquifers. Int J Hydrogen Energy 2023;48(69):26894–910. https://doi.org/10.1016/j.ijhydene.2023.03.363.
[53] Abdin Z, Tang C, Liu Y, Catchpole K. Large-scale stationary hydrogen storage via liquid organic hydrogen carriers. iScience 2021;24(9):102966. https://doi.org/10.1016/j.isci.2021.102966.
[54] Talukdar M, Blum P, Heinemann N, Miocic J. Techno-economic analysis of underground hydrogen storage in Europe. iScience 2024;27(1):108771. https://doi.org/10.1016/j.isci.2023.108771.
[55] Harati S, Gomari SR, Ramegowda M, Pak T. Multi-criteria site selection workflow for geological storage of hydrogen in depleted gas fields: a case for the UK. Int J Hydrogen Energy 2024;51(A):143–57. https://doi.org/10.1016/j.ijhydene.2023.10.345.
[56] National network of regional coastal monitoring programmes. https://coastalmonitoring.org/realtimedata. [Accessed 7 July 2025].
[57] UK marine renewables atlas. https://www.renewables-atlas.info/explore-the-atlas. [Accessed 7 July 2025].
[58] Recalde L, Yue H, Leithead W, Anaya-Lara O, Liu H, You J. Hybrid renewable energy systems sizing for offshore multi-purpose platforms. In: Proceedings of the ASME 2019 38th International Conference on Ocean, Offshore and Arctic Engineering (OMAE2019). Glasgow, UK: ASME; June . https://doi.org/10.1115/OMAE2019-96017. OMAE2019-96017, V010T09A059.
[59] Egeland-Eriksen T, Jensen JF, Ulleberg Ø, Sartori S. Simulating offshore hydrogen production via PEM electrolysis using real power production data from a 2.3 MW floating offshore wind turbine. Int J Hydrogen Energy 2023;48(74):28712–32. https://doi.org/10.1016/j.ijhydene.2023.03.471.
[60] Serna Á, Tadeo F. Offshore hydrogen production from wave energy. Int J Hydrogen Energy 2014;39(3):1549–57. https://doi.org/10.1016/j.ijhydene.2013.04.113.
[61] Bonacina CN, Gaskare NB, Valenti G. Assessment of offshore liquid hydrogen production from wind power for ship refueling. Int J Hydrogen Energy 2022;47(2):1279–91. https://doi.org/10.1016/j.ijhydene.2021.10.043.
[62] Yudwong B, Guilbert D, Phattanasak M, Kaewmanee W, Hinaje M, Vitale G. Faraday's efficiency modeling of a proton exchange membrane electrolyzer based on experimental data. Energies 2020;13(18):4792. https://doi.org/10.3390/en13184792.